



**HAL**  
open science

## 4D Printing Nanocomposite Hydrogel Based on PNIPAM and Prussian Blue Nanoparticles Using Stereolithography

Tristan Pelluau, Thomas Brossier, Michel Habib, Saad Sene, Gautier Félix,  
Joulia Larionova, Sébastien Blanquer, Yannick Guari

► **To cite this version:**

Tristan Pelluau, Thomas Brossier, Michel Habib, Saad Sene, Gautier Félix, et al.. 4D Printing Nanocomposite Hydrogel Based on PNIPAM and Prussian Blue Nanoparticles Using Stereolithography. *Macromolecular Materials and Engineering*, 2023, 309 (3), 10.1002/mame.202300305 . hal-04642801

**HAL Id: hal-04642801**

**<https://hal.science/hal-04642801v1>**

Submitted on 10 Oct 2024

**HAL** is a multi-disciplinary open access archive for the deposit and dissemination of scientific research documents, whether they are published or not. The documents may come from teaching and research institutions in France or abroad, or from public or private research centers.

L'archive ouverte pluridisciplinaire **HAL**, est destinée au dépôt et à la diffusion de documents scientifiques de niveau recherche, publiés ou non, émanant des établissements d'enseignement et de recherche français ou étrangers, des laboratoires publics ou privés.

# 4D Printing Nanocomposite Hydrogel Based on PNIPAM and Prussian Blue Nanoparticles Using Stereolithography

Tristan Pelluau, Thomas Brossier, Michel Habib, Saad Sene, Gautier Félix, Joulia Larionova, Sébastien Blanquer,\* and Yannick Guari\*

The potential of photoactive Prussian blue nanoparticles dispersed in thermo-responsive PNIPAM hydrogels in 4D printing using a stereolithography is investigated with digital light processing. The proportion of Prussian blue nanoparticles used in the resin is chosen to deliver a significant photothermal effect providing a heating above the volume phase transition temperature of the final nanocomposite hydrogels; while, giving only a limited effect on light scattering during the 3D printing process. Four formulations with various amounts of Prussian blue nanoparticles are used to print 3D structures with different shapes, such as Aztec pyramids, cylinders, gyroid porous cubes, and porous films. The shrinkage effect triggered by light irradiation at 808 nm on the as-obtained nanocomposite hydrogels is demonstrated through the delivery of a representative molecule fluorescein and a triggered 4D shape-morphing effect.

once a volume phase transition temperature (VPTT) is reached. The class of polymers with a low critical solution temperature (LCST) is the most investigated among the thermo-responsive hydrogels. Typically, LCST polymers display a thermodynamic change causing precipitation above the critical temperature. Few types of smart hydrogels based on LCST polymers have been investigated in the literature, but the number of works devoted to hydrogels based on poly(*N*-isopropylacrylamide (PNIPAM) is dominating due to its characteristic sharp LCST around 32 °C,<sup>[1]</sup> which evidences the potential for biomedical applications.<sup>[2,3]</sup> For instance, anisotropic deformations through thermal stimulation of PNIPAM based hydrogels have been notably used to create hydrogel actuators.<sup>[4,5]</sup>

## 1. Introduction

Hydrogels are a class of soft and elastic polymers with remarkable capacity to absorb a large amount of water. Such aptitude to swell in the presence of water leads to specific deformations of the hydrogel shape. Consequently, a reversible deformation process can be expected once water is expelled. In the case of smart hydrogels, the generated volume transformations can be triggered in time upon external stimulation. The behavior is a consequence of a phase transition within the polymer matrix, which alters its affinity with water. This ability is commonly encountered with smart thermo-responsive hydrogels, which can lead to a significant deformation by swelling/shrinking process

Recently, an important effort has been done on improving of the PNIPAM performance regarding its mechanical properties and the possibility of the shape control.<sup>[6]</sup> In this line of thought, the introduction of inorganic nanoparticles leading to smart nanocomposite hydrogels with unusual properties has been reported in the literature.<sup>[7]</sup> In particular, nanocomposite PNIPAM based hydrogel combined with nanoparticles is able to provide a local photothermic effect under light irradiation; and therefore, trigger the deformation by an orthogonal stimulation having captured a specific attention. Recent works presented such orthogonal thermo-stimulated PNIPAM hydrogels using nanoparticles, such as plasmonic gold nanorods,<sup>[8]</sup> nanothylakoid particles,<sup>[9]</sup> or graphene oxide.<sup>[10–12]</sup> Complex bilayer actuators have been developed with these smart nanocomposite hydrogels leading to efficient anisotropic near infra-red (NIR) light deformations.

Upgrading from 2D to 3D structures involves the use of additive manufacturing approaches.<sup>[13]</sup> Smart PNIPAM nanocomposite hydrogel in 4D printing technology remains a pristine field and a challenging task. The 4D printing is a recent process, which consists in modifying functions, properties or shapes of externally stimulable 3D objects fabricated by additive manufacturing. The literature on the development of smart hydrogels through 4D printing using stereolithography is quite scarce.<sup>[14–19]</sup> Moreover, to the best of our knowledge, there are no reports on the creation of smart nanocomposite hydrogels using this particular technique. Interestingly, no research has been carried out thus far to investigate the incorporation of Prussian blue nanoparticles into 3D printed hydrogel nanocomposites.

T. Pelluau, T. Brossier, M. Habib, S. Sene, G. Félix, J. Larionova, S. Blanquer, Y. Guari  
 ICGM, University Montpellier  
 CNRS, ENSCM  
 1919 route de Mende, Montpellier 34000, France  
 E-mail: sebastien.blanquer@umontpellier.fr;  
 yannick.guari@umontpellier.fr

 The ORCID identification number(s) for the author(s) of this article can be found under <https://doi.org/10.1002/mame.202300305>

© 2023 The Authors. Macromolecular Materials and Engineering published by Wiley-VCH GmbH. This is an open access article under the terms of the Creative Commons Attribution License, which permits use, distribution and reproduction in any medium, provided the original work is properly cited.

DOI: 10.1002/mame.202300305

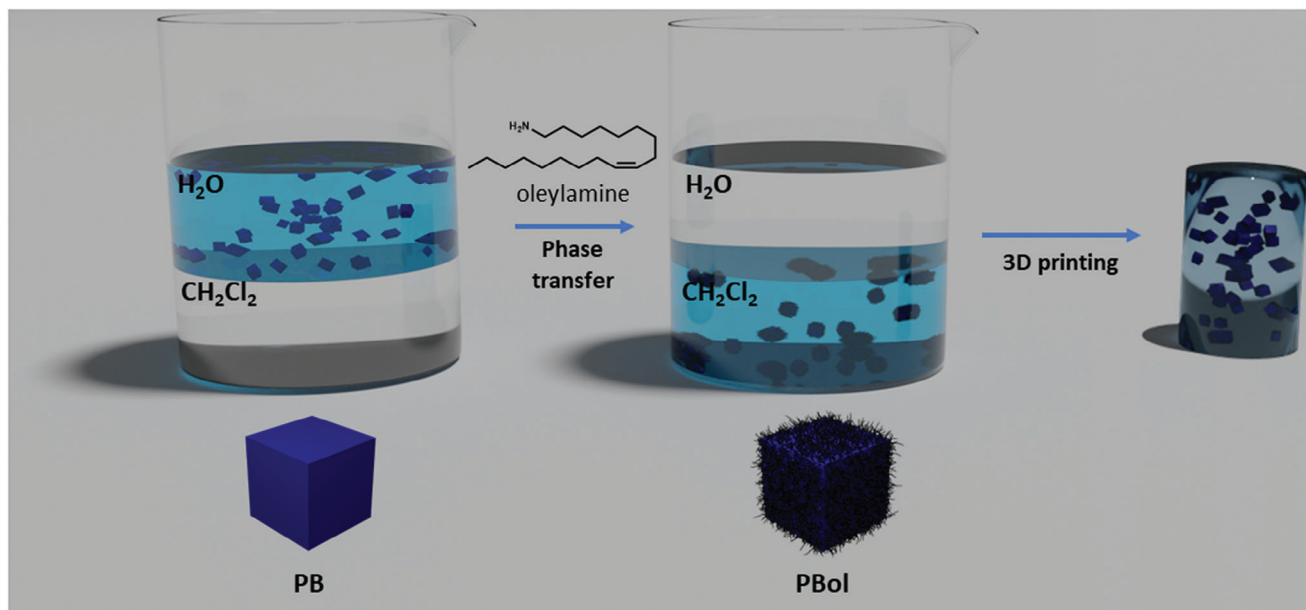


**Figure 1.** Schematic representation of the synthesis of PB and PBol nanoparticles and the fabricated nanocomposite hydrogels by DLP stereolithography.

Prussian blue (PB) presents a chemical formula  $A_{1-x}Fe^{III}[Fe^{II}(CN)_6]_{1-x/4}\square_{x/4}\cdot nH_2O$ , where  $n$  is the number of water molecules,  $A$  is a monovalent cation, and  $\square$  is a cyanometallate vacancy needed to assure the electroneutrality. In its crystal structure, the  $Fe^{2+}$  and  $Fe^{3+}$  ions are linked through cyano-bridges to form a porous 3D face centered cubic structure (*fcc*).<sup>[20–24]</sup> The development of PB nanoparticles has been initiated recently with two pioneering works reported by S. P. Moulik et al. in 1999<sup>[25]</sup> and S. Mann et al. in 2000.<sup>[26]</sup> Starting with these seminal works, the synthesis and investigation of nano-sized PB systems have attracted a great deal of attention from numerous research teams worldwide.<sup>[27–32]</sup> The amazing prospects offered by PB nano-objects in comparison to other inorganic nano-sized systems consist in the fact that they present a variety of useful properties among which their photothermal activity takes an important place. In fact, PB nanoparticles have an intense absorption band in the NIR between 600 and 900 nm with a high molar extinction coefficient of  $1.2 \times 10^{11} \text{ m}^{-1} \text{ s}^{-1}$ , providing an exceptional photothermal conversion effect of up to 41.4%, which can be compared to the reference nano-objects in this area, such as the gold nanorods (21%) or gold nanovesicles (37%), but with better photothermal stability.<sup>[33]</sup> Therefore, these nanoparticles are able to provide an important and localized temperature rise when subjected to irradiation in the NIR domain, which is suitable for various applications in the biomedical field.

We therefore propose in this study to investigate the potential of photoactive PB nanoparticles dispersed in thermo-responsive PNIPAM hydrogels in 4D printing process using a stereolithography process with digital light processing (DLP). DLP stereolithography is an additive manufacturing process that has already demonstrated its efficiency to fabricate sophisticated 3D structures with a remarkable precision.<sup>[34,35]</sup> The principle is based on spatial curing layer-by-layer of a photo-printable polymer resin.<sup>[36]</sup> Using this approach, we intend to develop a smart photothermal-responsive composite hydrogel using NIR

stimulation to generate localized deformation and release of molecules.

## 2. Results and Discussion

### 2.1. Synthesis and Characterization of PB and PBol Nanoparticles

First, PB (Prussian blue) nanoparticles were synthesized through the controlled addition of  $Fe^{3+}$  and hexacyanoferrate  $Na_4[Fe(CN)_6]$  building blocks using a peristaltic pump in an aqueous media as previously reported (Figure S1, Supporting Information).<sup>[37–39]</sup> The as-obtained PB nanoparticles were then covered with oleylamine using a phase transfer protocol to obtain PBol (prussian blue oleylamine) nanoparticles (Figure 1).<sup>[40]</sup>

The IR spectra were recorded especially in the spectral window 1800–2400  $\text{cm}^{-1}$ , that is, in the vicinity of the  $CN^-$  stretching modes, which are fingerprints of the structural and electronic changes occurring in cyano-bridged compounds (Figure S2, Supporting Information). Both PB and PBol exhibited a strong band at 2078  $\text{cm}^{-1}$ , which was characteristic of the stretching cyanide vibration,  $\nu(Fe^{II}-CN-Fe^{III})$  of PB. Further, both samples displayed the typical stretching and bending modes of the  $Fe^{II}-CN$  at 601 and 500  $\text{cm}^{-1}$ . In addition, the IR spectrum for PBol showed the stretching vibration bands  $\nu(C-H)$  and  $\nu(C=C)$  at 2800–3000  $\text{cm}^{-1}$  and 1655  $\text{cm}^{-1}$ , respectively, due to the presence of oleylamine. Both samples showed a strong adsorption band in their absorption spectra at 723 nm, which was due to a transition during which an electron was transferred from a ground state  $Fe_A(III)Fe_B(II)$  to an excited state  $Fe_A(II)Fe_B(III)$  form (Figure S3, Supporting Information).<sup>[41]</sup>

The X-ray diffraction pattern obtained for nanoparticles PB and PBol are characteristic of the *fcc* PB structure with cell parameters of 10.1656(2) Å and 10.2032(3) Å, respectively (Figure S4, Supporting Information). The crystallites' sizes obtained by using the Scherrer equation were equal to 110 and

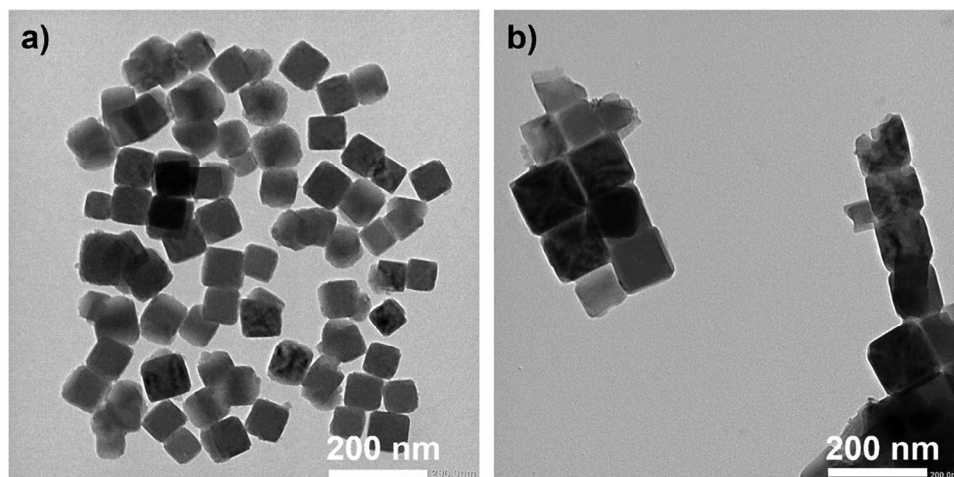


**Figure 2.** TEM images of a) PB and b) PBol nanoparticles.

85 nm for PB and PBol, respectively. The transmission electronic microscopy (TEM) images for PB and PBol showed well-defined cubic nanoparticles with sizes of  $111.2 \pm 12.2$  nm and  $107.9 \pm 13.8$  nm, respectively (Figure 2). The SEM/EDS coupled with TGA analysis for PB and PBol allowed obtaining the following formulas of  $\text{Na}_{0.32}\text{Fe}[\text{Fe}(\text{CN})_6]_{0.83}\square_{0.17} \cdot 10\text{H}_2\text{O}$  and  $\text{Na}_{0.33}\text{Fe}[\text{Fe}(\text{CN})_6]_{0.83}\square_{0.16} \cdot 3.8\text{oleylamine} \cdot 8.6\text{H}_2\text{O}$  for PB and PBol, respectively (Figure S5, Supporting Information). The ThermoGravimetric analysis (TGA) curves were carried out for oleylamine, PB, and PBol showing that the degradation of the PB structure occurred at a similar temperature for PB and PBol, that is  $\approx 250$  °C. However, while the degradation temperature of oleylamine occurred at 245 °C; it occurred at 434 °C within PBol, which could be explained by the interaction of oleylamine with PB nanoparticles' surface. Similar shift to higher degradation temperature has been observed on silver nanoparticles coated with oleylamine.<sup>[42]</sup>

## 2.2. Printability and Characterization of the Printed Nanocomposite Hydrogels

PNIPAM was widely used in the design of thermosensitive hydrogels due to its specific VPTT around 32–37 °C, resulting in a volume contraction of the hydrogel and water expulsion.<sup>[43]</sup> We investigated a nanocomposite resin based on *N*-isopropylacrylamide and PEG dimethacrylate as crosslinker where PB nanoparticles coated with oleylamine (PBol) had been added in different proportions (Figure 3). PB is known as an efficient photothermal agent that is used to reach VPTT of PNIPAM by simple appropriate light irradiation. However, given that PB is a natural blue pigment, the proportions should be carefully selected to ensure high-resolution printing by photopolymerization with limited light scattering. Different PNIPAM hydrogels have been prepared in the presence of PEGDA700 as crosslinker and Darocur 1173 as photoinitiator. We have then chosen four different formulations to generate nanocomposite hydrogels denoted as  $^{0.07}\text{PBol}$ ,  $^{0.12}\text{PBol}$ ,  $^{0.22}\text{PBol}$ , and  $^{0.30}\text{PBol}$  with increasing quantity of PBol nanoparticles given in mg of Fe per

gram (see Experimental Section). A reference hydrogel without PB nanoparticles denoted  $^0\text{PBol}$  was also elaborated in the same experimental conditions. The chosen range of PB amount ensured a significant increase in temperature under irradiation once the nanocomposite hydrogels had been produced, but on the other hand, it was low enough to avoid any influence in the printing process. SLA printing process was done with Asiga Max X with 43  $\mu\text{m}$  of XY resolution and 100  $\mu\text{m}$  layer thickness as obtained from the working curve shown in Figure S6, Supporting Information. Hence, all formulations required 10 s irradiation under 5  $\text{mW cm}^{-2}$  UV light to cure 100  $\mu\text{m}$  layer resin. By increasing the PBol nanoparticles' content, the characteristic blue colour intensified as it could be seen for the cylinders on top of Figure 3 (from left to right). In addition, five formulations were used in order to print various 3D structures such as Aztec pyramids, cylinders, gyroid porous cubes, and porous films (Figure 3). The PBol nanoparticles were easily dispersed in EG during formulation of the resin due to their hydrophobic coating. In addition, the hydrophobic coating on the nanoparticles enhanced their stability in the hydrogel matrix as no release was observed from the system after several months in water.

The IR spectra of the hydrogels  $^{0.07}\text{PBol}$ – $^{0.30}\text{PBol}$  showed the stretching and bending vibration bands for amine N–H bond at 3275 and 1538  $\text{cm}^{-1}$  and the stretching vibration mode for C=O bond at 1634  $\text{cm}^{-1}$  characteristic of PNIPAM (Figure S7, Supporting Information).<sup>[44]</sup> In addition, magnification in the spectral window 1800–2500  $\text{cm}^{-1}$  revealed the presence of the CN stretching vibration at  $\approx 2100$   $\text{cm}^{-1}$  for NH  $^{0.07}\text{PBol}$ – $^{0.30}\text{PBol}$ . Structures  $^{0.07}\text{PBol}$ – $^{0.30}\text{PBol}$  showed an adsorption band in their electronic spectra at  $\approx 771$  nm, which was typical of an electron transfer from a  $\text{Fe}_A(\text{III})\text{Fe}_B(\text{II})$  ground state to an  $\text{Fe}_A(\text{II})\text{Fe}_B(\text{III})$  excited state occurring in PB which was absent in the PB nanoparticles' free hydrogel  $^0\text{PBol}$  (Figure S8, Supporting Information). Both spectroscopies confirmed the successful integration of PB nanoparticles in the nanocomposite hydrogels  $^{0.07}\text{PBol}$ – $^{0.30}\text{PBol}$ . Finally, TEM images of  $^{0.30}\text{PBol}$  using ultramicrotomy technique showed that the PB nanoparticles formed homogeneously dispersed in the nanocomposite hydrogel islands of few nanoparticles (Figure S9, Supporting

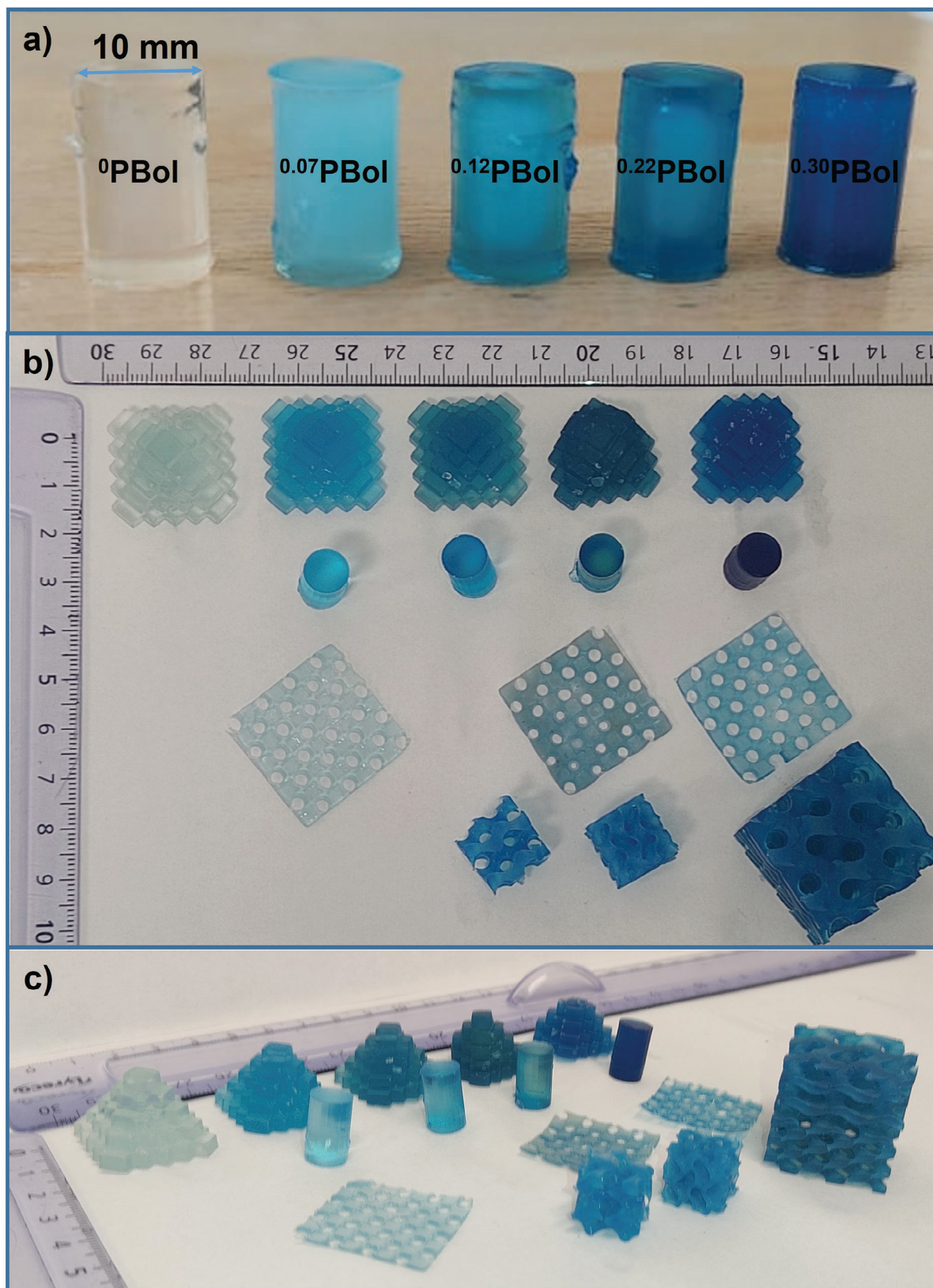


**Figure 3.** Photographs of nanocomposite hydrogel containing PB nanoparticles: a) side view of cylinders, b) top view, and c) perspective view for a selection of swollen 3D-printed structures in the shape of Aztec pyramids, cylinders, gyroid porous cubes, and porous films with increasing PBol concentration from left to right.

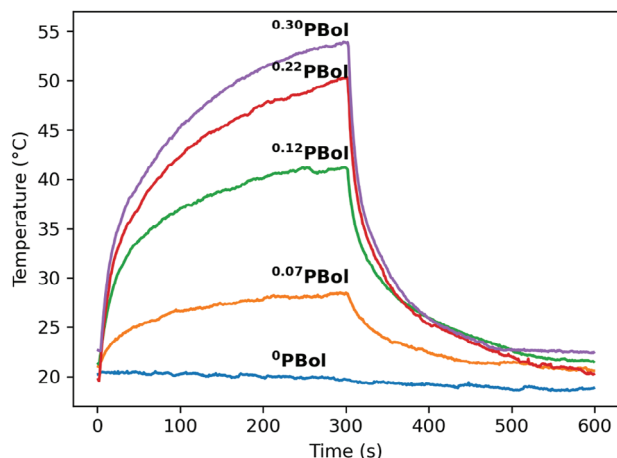


**Figure 4.** Photothermal experiments for 3D printed hydrogels in the shape of cylinders  $^0\text{PBol}$  (blue),  $^{0.07}\text{PBol}$  (orange),  $^{0.12}\text{PBol}$  (green),  $^{0.22}\text{PBol}$  (red), and  $^{0.30}\text{PBol}$  (purple) under irradiation at 808 nm.

Information). The characteristic VPTT for the thermosensitive hydrogels  $^0\text{PBol}$ – $^{0.30}\text{PBol}$  was measured by Differential Scanning Calorimetry (Figure S10, Supporting Information). It could be seen from the thermograms that all the investigated hydrogels showed similar thermal response between 10 °C and 60 °C. The VPTT was detected between 28 °C and 40 °C with a PNIPAM characteristic peak between 33 °C and 35 °C. Therefore, the presence of PB nanoparticles did not influence the VPTT of PNIPAM based hydrogels. It is known that the addition of inorganic particles in a polymer matrix with specific proportion and size tends to reinforce the mechanical performance of the final composite material.<sup>[45–47]</sup> In this line, we studied the mechanical behaviour of the hydrogels under compression and shear stresses. For both studies, the incorporation of nanoparticles within the PNIPAM based hydrogels did not show any significant difference in the compression and shear stress moduli (Figure S11, Supporting Information). In fact, Young's modulus was found to be  $\approx 14$  kPa across all samples. Similarly, by rheological measurements, all samples showed similar  $G'$  and  $\tan \delta$  of 250 Pa and 0.04, respectively. It can be concluded that the proportion of nanoparticles in all nanocomposite hydrogels was sufficiently low to not influence their thermal response nor their mechanical properties.

### 2.3. Photothermal Effect on Printed Structures

The photothermic effect in the nanocomposite hydrogels was investigated by using a thermal camera for monitoring the temperature modification over 5 min' irradiation under at 808 nm. **Figure 4** shows the temperature variation versus time for the nanocomposite  $^{0.07}\text{PBol}$ – $^{0.30}\text{PBol}$  hydrogel cylinders taking the printed cylinder without PB nanoparticles as a reference. While the reference hydrogel without PB nanoparticles didn't show any temperature increase, it could be seen that the temperature increased when the amount of PB nanoparticles in the nanocomposite hydrogels increased reaching a plateau with maximum temperature of 28.4 °C, 41.1 °C, 50.3 °C, and 53.9 °C for  $^{0.07}\text{PBol}$ ,  $^{0.12}\text{PBol}$ ,  $^{0.22}\text{PBol}$ , and  $^{0.30}\text{PBol}$ , respectively (Figure S12, Supporting Information). This study demonstrates that the proportion of

PB nanoparticles used in the resin is sufficient to deliver a significant photothermal effect allowing the heating above the VPTT of the nanocomposite hydrogels when the amount of PB is equal or superior to 0.08 mg of Fe per g of nanocomposite (nanocomposite hydrogel  $^{0.12}\text{PBol}$ ).

Nanocomposite hydrogel  $^{0.30}\text{PBol}$  was selected due to its efficient photothermal effect for further studies on simple 3D printed cubes. To do so, the top face of simple 3D printed cubes ( $5 \times 5 \times 5$  mm) of  $^{0.30}\text{PBol}$  was irradiated with NIR light for 15 min (**Figure 5a**). Upon irradiation, the nanocomposite hydrogel noticeably shrunk (**Figure 5b**) and water was expelled from the matrix. This volume change corresponded to the heat dissipation in the hydrogel due to the photothermal effect from the PB nanoparticles absorbing the NIR light and transforming it into heat. The successful shrinkage of the nanocomposite hydrogel confirmed that the amount of PB nanoparticles was sufficient to induce an increase of the temperature above the VPTT. In order to evaluate the volume change, the residual mass for  $^{0.30}\text{PBol}$  was measured after 15-, 30-, and 60-min. of irradiation. The residual mass represents the nanocomposite hydrogel mass after the expulsion of water upon irradiation. A significant water loss of 36%, 48%, and 60% was detected after 15, 30, and 60 min of irradiation, respectively. The same experiment was also performed with the PB nanoparticles' free hydrogel  $^0\text{PBol}$  as a reference. In that case, the water loss was relatively low and reached 7%, 14%, and 20% after irradiation during 15, 30, and 60 min. This latter could be attributed to the dehydration of the hydrogel in ambient atmosphere, the VPTT not being reached in that case. Note that the quantity of water expressed in % refers to the maximum mass loss during the elimination of water for the corresponding nanocomposite hydrogel dried in an oven for 12 h at 100 °C (Figure S13, Supporting Information). This difference in behaviour of  $^0\text{PBol}$  and  $^{0.30}\text{PBol}$  under NIR irradiation demonstrated the effect of PB nanoparticles where the photothermal effect triggered the shrinkage of the hydrogel resulting in the water expulsion. Once the irradiation was stopped, the shrunken printed cube was placed in an aqueous medium at room temperature where it recovered its original volume after at least 30 min through water reabsorption (**Figure 5c**). The significant loss of water observed for  $^{0.30}\text{PBol}$  and the related deformation on an irradiated object in its entirety shows the advantage of this type of material with a very significant deformation/collapse. In addition, carrying out heating and then rehydration cycles beyond three cycles did not show any material fatigue with a preserved shape and constant loss and rehydration rates (**Figure S14**, Supporting Information).

The volume change observed upon irradiation could be used as a tool to induce shape deformation of 3D printed structures. For instance, taking a 3D printed staircase (**Figure 5d**), the dimensions of a single step could be modified by irradiating the chosen area (Movie S1, Supporting Information). As shown in **Figure 5**, only the irradiated zone of a staircase-based hydrogel  $^{0.30}\text{PBol}$  shrunk (**Figure 5e**). In addition, the expelled water droplet could be seen flowing on the side. As previous, this shape deformation could be recovered upon submerging the deformed structure in aqueous solution at room temperature (**Figure 5f**).

Following the demonstration of the localized shrinkage of the printed structure after NIR irradiation and its promise in 4D printing, we also intended to demonstrate the potential of

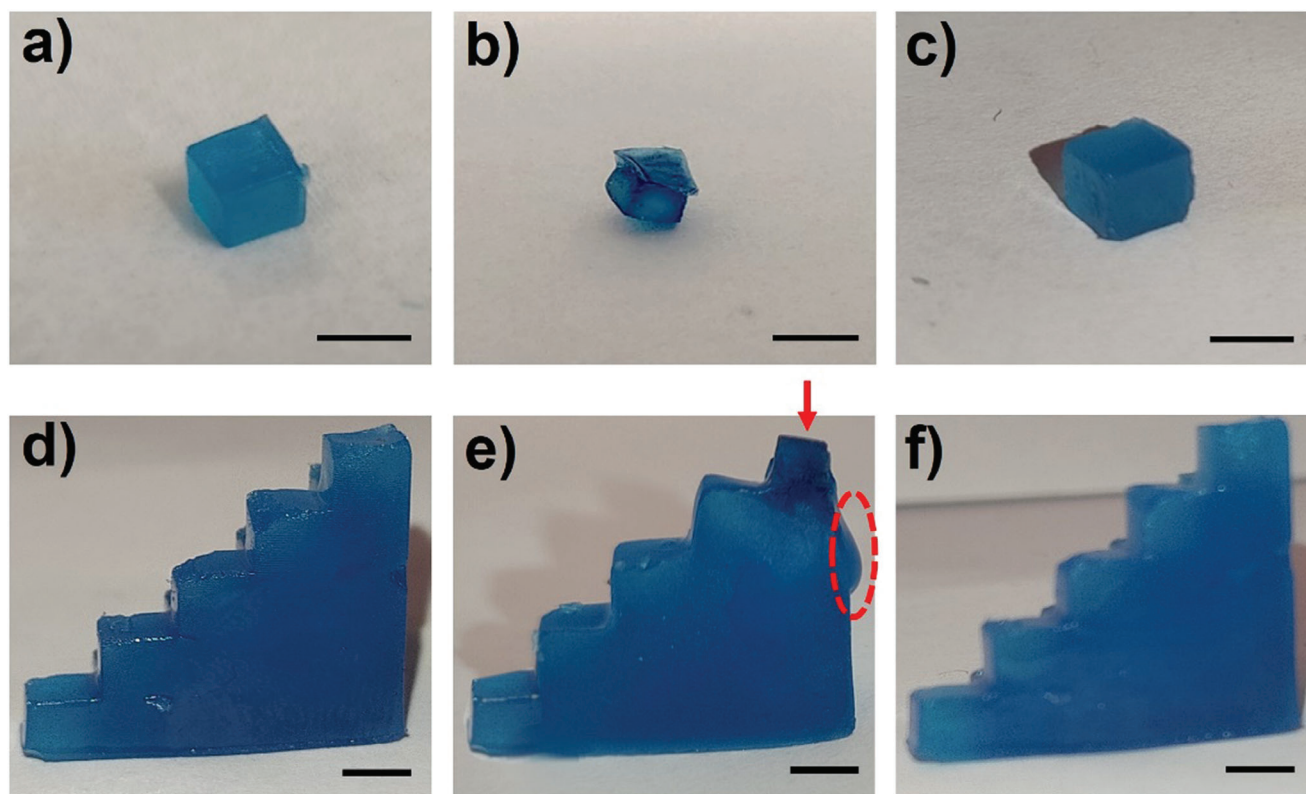


**Figure 5.** Visual aspect of 3D-printed cube and staircase nanocomposite hydrogel  $^{0.30}$ PBoI a,d) before; b,e) after 60 min of irradiation by a laser at 808 nm; and c,f) after at least 30 min in water. The arrow shows the irradiated area and the dotted circle indicates the formed water droplet. Scale bar = 5 mm.

our approach in delivery of molecules in solution. To this purpose, fluorescein sodium salt was chosen as a hydrophilic drug model loaded in a 3D printed structure in order to investigate its delivery under NIR irradiation. After impregnating  $^{0.30}$ PBoI with fluorescein, the hydrogel's colour changed from blue to green which was the characteristic color of fluorescein sodium salt as it could be seen in **Figure 6a,b**. The amount of fluorescein impregnated was 0.011 mmol per gram of nanocomposite hydrogel  $^{0.30}$ PBoI.

A sample of  $^{0.30}$ PBoI loaded with fluorescein was placed in water and irradiated locally during 10 min on a small cubic outgrowth, as shown by the arrow of **Figure 6d** (in the same manner as shown in **Figure 3**). For comparison, a reference sample  $^{0.30}$ PBoI loaded with fluorescein was placed in water for 10 min without irradiation (**Figure 6c**). In both cases, the supernatant's colour became yellowish (**Figure 6e,f**). From **Figure 6g**, it could be seen that both supernatants showed the presence of the characteristic absorption peak of fluorescein at 490 nm. By using the spectrophotometric calibration curve of fluorescein, its delivery was measured without and after irradiation in solution at 808 nm. The release of fluorescein corresponded to 9% and 16% of the total amount incorporated in sample 5 without and with irradiation, respectively. This increase in release in solution may be explained thanks to a temperature rise of the hydrogel in the irradiated zone which, compared to the non-irradiated sample, enhanced the diffusion mechanism. It could be concluded that the spatially controlled volume transformation could be used as

a means to induce shape deformation as a solid, as well as to release encapsulated molecules in a liquid.<sup>[48,49]</sup>

It should be noted that the amplitude of the deformation will depend on the shape of the hydrogel nanocomposite. When a nanocomposite hydrogel  $^{0.30}$ PBoI 3D-printed as a square grid containing fluorescein was irradiated at 808 nm for 2 min at each square of the grid following a diagonal shown as a blue arrow on **Figure 7b**, the resulting nanocomposite hydrogel (**Figure 7c**) displayed a considerably altered shape compared to its initial flat form (**Figure 7a**) (Movie S2, Supporting Information). In the irradiated area, the surface of the film shrunk first, creating a swelling gradient across its thickness; creating therefore, a mechanical stress between the shrunk and the swollen parts and forcing the system to bend. Thus, by the integration of PB nanoparticles in a PNIPAM matrix, a photothermal response was added to the system triggering the 4D shape-morphing effect upon NIR irradiation demonstrating the possibility to design through DLP stereolithography PB-based nanocomposite hydrogels as potential remotely activated actuators.

### 3. Conclusion

We elaborated nanocomposite hydrogels associating photoactive PB nanoparticles with a thermo-responsive matrix, PNIPAM via a DLP stereolithography process. To do so, the PB nanoparticles were coated with oleylamine conferring them a hydrophobic

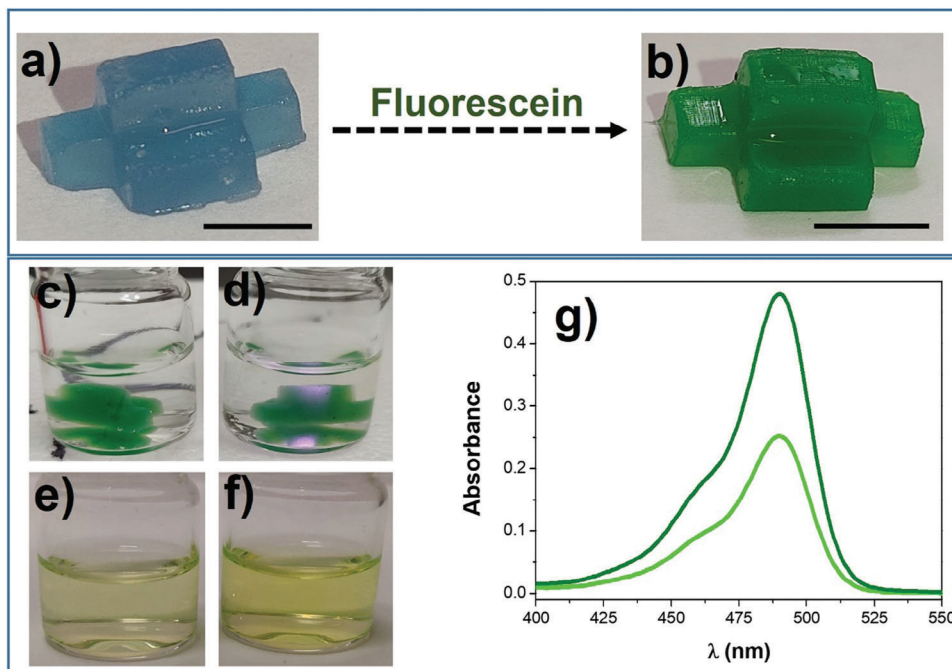


**Figure 6.** Photographs of the 3D-printed polymer: a) before and b) after impregnation in a fluorescein solution for one night, placed in 2 mL of water for 10 min. c) Without and d) with irradiation and e, f) their respective supernatants after removal of  $^{0.30}$ PBol. g) UV-vis spectra of the supernatants for the experiment without irradiation (light green) and with laser irradiation at 808 nm (dark green). Scale bar = 5 mm.

coating allowing easy dispersion during formulation of the resin and a good affinity for the hydrogel matrix avoiding any release in water even for several months in water. Moreover, during all the irradiation experiments inducing a deformation of the structure induced by shrinkage, we never observed any release of the PB nanoparticles either. The PB proportions were selected considering high-resolution printing by photo-polymerization with limited light scattering and efficiency for photothermal effect in the aim to reach temperatures above the VPTT of the nanocomposite hydrogels.

The 3D printability was demonstrated for all formulations tested obtaining various 3D structures. Further, the temperature increase of the nanocomposite hydrogels upon irradiation at 808 nm was measured and demonstrated a correlation between

the quantities of PB nanoparticles inserted in the nanocomposite. The minimum amount of PB nanoparticles to reach the VPTT of the nanocomposite was then determined. The photothermal effect of hydrogels was then used to produce the localized shrinkage and the controlled water expulsion. This process was shown to be fully reversible by immersing the nanocomposite hydrogels in water at room temperature. Such phenomenon was also exploited to demonstrate the possibility to trigger delivery of a drug molecule model, fluorescein sodium salt, which was previously loaded in the nanocomposite hydrogel. Finally, depending on the shape of the nanocomposite hydrogels, it was shown that its deformation under laser irradiation could be accentuated leading to potential remotely activated actuators. This type of nanocomposite hydrogel represents an interesting example of

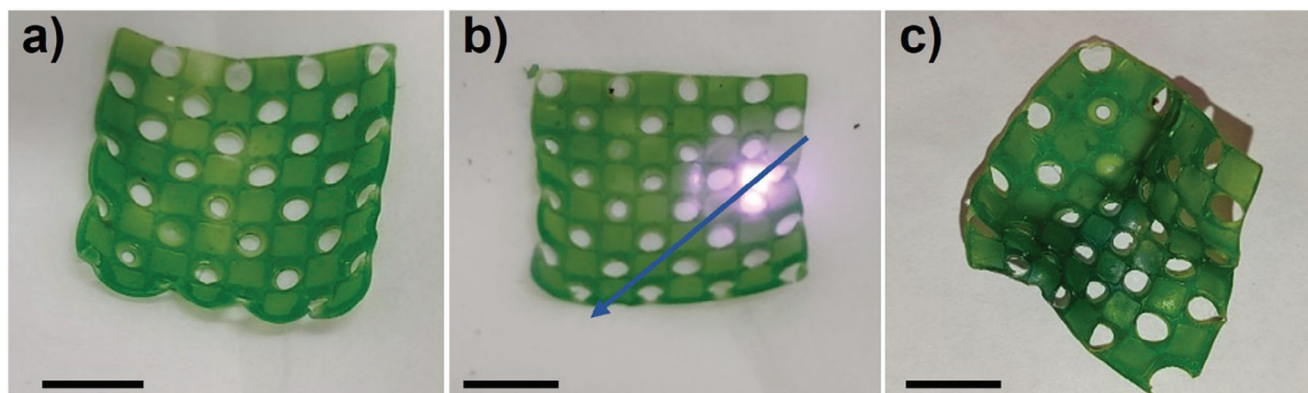


**Figure 7.** Photographs of the 3D-printed nanocomposite hydrogel  $^{0.30}$ PBol square grid containing fluorescein a) before irradiation; b) during irradiation with a laser at 808 nm following the blue arrow for 2 min at each square; and c) final shape after irradiation. Scale bar = 1 cm.

thermosensitive 4D nanocomposites, in particular for their potential in the field of medical devices.

#### 4. Experimental Section

**Chemicals:** All chemical reagents were purchased and used without further purification. Sodium hexacyanoferrate(II) decahydrate (Alfa Aesar, 99%), iron(III) chloride hexahydrate (Sigma–Aldrich, 97%), ultrapure water (resistivity 18.2 MΩ.cm), oleylamine (Acros Organics, 80–90%), fluorescein (Acros organics, pure), dichloromethane (Merck, ACS), 2-hydroxy-2-methylpropiophenone (Darocur 1173, Sigma–Aldrich), N-isopropylacrylamide (NIPAM, Sigma–Aldrich 97.0%), poly(ethylene glycol) diacrylate, (PEGDA<sub>700</sub>, Sigma–Aldrich 97.0%), and ethylene glycol were commercial products and used without further purification.

**Synthesis of Prussian Blue Nanoparticles (PB):** The PB nanoparticles were synthesized using a controlled co-precipitation method adapted from a previously reported method leading to the formation of cubic shape nanoparticles.<sup>[37–39]</sup> Na<sub>4</sub>[Fe(CN)<sub>6</sub>]·10H<sub>2</sub>O at 11.25 mM and FeCl<sub>3</sub>·6H<sub>2</sub>O at 10 mM in water were simultaneously added at 25 °C using thermostatically controlled beakers at a speed of 4 mL h<sup>-1</sup> using a peristaltic pump for 10 h (40 mL in a total of each solution) in a dead volume of 100 mL of water. The final suspension was collected by centrifugation at 37500 × g (20 000 rpm, 15 min). The final nanoparticles were obtained after three cycles of centrifugation/water washing.

IR (ATR):  $\nu(\text{O—H}) = 3235 \text{ cm}^{-1}$  (crystallized water),  $\nu(\text{C}\equiv\text{N}) = 2078 \text{ cm}^{-1}$  (PB),  $\delta(\text{O—H}) = 1611 \text{ cm}^{-1}$  (crystallized water),  $\nu(\text{Fe}^{\text{II}}\text{—CN}) = 601 \text{ cm}^{-1}$  (PB),  $\delta(\text{Fe}^{\text{II}}\text{—CN}) = 500 \text{ cm}^{-1}$  (PB); EDS: Na/Fe = 0.17; TGA: 50.6% at 800 °C; Estimated formula: Na<sub>0.32</sub>Fe[Fe(CN)<sub>6</sub>]<sub>0.83</sub>□<sub>0.17</sub>·10H<sub>2</sub>O;  $d_{\text{TEM}} = 111.2 \pm 12.2 \text{ nm}$ ; UV:  $\lambda_{\text{max}} = 723 \text{ nm}$ ;  $m = 100 \text{ mg}$ ; Yield: 94%.

**Prussian Blue Nanoparticles Coating by Oleylamine (PBol):** The PB nanoparticles were coated with a layer of oleylamine to transfer them in an organic phase through liquid–liquid separation. 50 mg of PB nanoparticles was dispersed in 10 mL of water and separately, 100 mL of dichloromethane was mixed with 5 mL of oleylamine. Several PB nanoparticles extraction was performed by stirring the aqueous phase and 10 mL of the organic phase for a few min followed by a liquid–liquid separation. All the organic phases were collected and centrifuged at 37500 × g (20 000 rpm, 15 min).

IR (ATR):  $\nu(\text{O—H}) = 3235 \text{ cm}^{-1}$  (crystallized water),  $\nu(\text{C—H}) = 2800\text{–}3000 \text{ cm}^{-1}$  (oleylamine),  $\nu(\text{C}\equiv\text{N}) = 2078 \text{ cm}^{-1}$  (PB),  $\nu(\text{C=C}) = 1655 \text{ cm}^{-1}$  (oleylamine),  $\delta(\text{O—H}) = 1611 \text{ cm}^{-1}$  (crystallized water),  $\nu(\text{Fe}^{\text{II}}\text{—CN}) = 601 \text{ cm}^{-1}$  (PB),  $\delta(\text{Fe}^{\text{II}}\text{—CN}) = 500 \text{ cm}^{-1}$  (PB); EDS: Na /Fe = 0.19; TGA: 16.4% at 800 °C; Estimated formula: Na<sub>0.33</sub>Fe[Fe(CN)<sub>6</sub>]<sub>0.83</sub>□<sub>0.16</sub> 3.8oleylamine·8.6H<sub>2</sub>O;  $d_{\text{TEM}} = 107.9 \pm 13.8 \text{ nm}$ ; UV:  $\lambda_{\text{max}} = 723 \text{ nm}$ ;  $m: 87 \text{ mg}$ ; Yield: 15%.

**Photo-Sensitive Resins Formulations and Fabrication of 3D Printed Objects 1 and 2–5 by SLA:** The resins formulations were prepared by dissolving PEGDA700 (3 wt% relative to the formulation) and NIPAM (50 wt% relative to the formulation) in ethylene glycol (47 wt%) as a non-reactive diluent. Then nanoparticles were added to the formulations at different proportions in PB (0.4 mg.g<sup>-1</sup>; 0.7 mg.g<sup>-1</sup>; 1.1 mg.g<sup>-1</sup>; 1.5 mg.g<sup>-1</sup>). Finally, darocur 1173 (3 wt% relative to the polymer) was added as photoinitiator. The solutions were stirred and sonicated few min to allow homogeneous photo-polymerization and provided an efficient cure depth and optimal pattern resolution.

3D structures were designed using the STL format of Rhinoceros 3D. The 3D structures were constructed from the mentioned resins by stereolithography at 385 nm (Max X27, Asiga Australia). The 3D objects were constructed by photo-crosslinking successive layers of resin with a thickness of 100 μm. This optimal layer thickness was determined using the Jacob's equation. Each layer was irradiated at an intensity of 5 mW cm<sup>-2</sup> for 10 s. After construction, the structures were removed from the stage and washed with distilled water for 24 h to eliminate unreacted prepolymer residues.

IR (ATR):  $\nu(\text{N—H}) = 3275 \text{ cm}^{-1}$  (PNIPAM),  $\nu(\text{C—H}) = 2800\text{–}3000 \text{ cm}^{-1}$  (PNIPAM),  $\nu(\text{C}\equiv\text{N}) = 2100 \text{ cm}^{-1}$  (PB),  $\nu(\text{C=O}) = 1634 \text{ cm}^{-1}$  (PNIPAM),

$\delta(\text{N—H}) = 1538 \text{ cm}^{-1}$  (PNIPAM);  $d_{\text{TEM}} \approx 94 \pm 15 \text{ nm}$ ; UV:  $\lambda_{\text{max}} = 771 \text{ nm}$ ; Fe Elementary analysis (ppm): 0.07 for <sup>0.07</sup>PBol, 0.12 for <sup>0.12</sup>PBol, 0.22 for <sup>0.22</sup>PBol and 0.30 for <sup>0.30</sup>PBol.

**Characterizations:** Transmission electron microscopy (TEM) images were performed at 100 kV (JEOL 1200 EXII). Samples for TEM measurements were deposited from suspensions on copper grids and allowed to dry before observation. The size distribution histograms of PB and PBol nanoparticles were determined using enlarged TEM micrographs taken at magnification of 100 K on a statistical sample of ≈100 nanoparticles. Slices of ≈60–100 nm of the nanocomposite <sup>0.30</sup>PBol were cut with an ultramicrotome apparatus equipped with a diamond knife allowing visualization of the PBol nanoparticles. SEM/EDS microscopy was performed on a FEI Quanta FEG 200 instrument. The powders were deposited on an adhesive carbon film and analyzed under high vacuum. The quantification of the heavy elements was carried out with the INCA software, with a dwell time of 3 μs. The amount of iron in the nanocomposite hydrogels <sup>0.07</sup>PBol–<sup>0.30</sup>PBol was determined using ICP-AES (Spectro Arcos ICP, AMETEK Materials Analysis). The nanocomposites were dried prior to digestion (≈140 mg of nanocomposites <sup>0.07</sup>PBol, <sup>0.12</sup>PBol, <sup>0.22</sup>PBol, and <sup>0.30</sup>PBol) in 100 μL of HNO<sub>3</sub> (67–69% super pure for trace analysis); and then, diluted in 10 mL of ultrapure H<sub>2</sub>O. Infrared spectra were obtained by attenuated total reflectance (ATR) on a PerkinElmer Spectrum Two spectrophotometer with four acquisitions at a resolution of 4 cm<sup>-1</sup>. UV–visible spectra (UV–vis) were collected on a V-650 spectrophotometer model from JASCO. DSC analysis were carried out using a Mettler Toledo (Mettler Toledo, France) DSC1 calorimeter. A constant calibration was performed with standards of biphenyl, indium, bismuth, zinc, and cesium chloride standards. Nitrogen was used as the purge gas. For the measurements, in order to detect a signal in DSC, the samples were analysed at a semi-swollen state with 50% w/w of water. 40 mg of swollen gels was put in a high-pressure aluminium sample holder (120 μL). Thermal properties were recorded between 10 °C and 60 °C at a heating rate of 5 °C min<sup>-1</sup> at the second cycle.

**Photothermal Measurements:** The photothermal properties of the nanocomposites were measured using two different setups. LASER setup: The samples were irradiated by a laser (Kamax society, Limoges, France) at 808 nm with a diameter of 1 cm and an adjustable light surface power from 0 to 2.58 W cm<sup>-2</sup> for a chosen time. The laser spot surface was 0.32 cm<sup>2</sup>. The temperature variations were measured using a thermal camera.

**Contraction and Release Measurements:** Nanocomposites with different size and shape with or without PB nanoparticles were irradiated for 60 min with the LASER setup. The contraction of the polymers was followed by monitoring their mass every 15 min, and pictures were taken at the beginning and the end of the experiment. After one hour of irradiation, the samples were left in water for at least 30 min, and a picture as well as their mass is taken the following day.

**Hydration/Dehydration Cycles Experiment:** A rectangular cuboid of <sup>0.22</sup>PBol with a (hydrated) volume of 92 mm<sup>3</sup> was utilized to carry out hydration/dehydration cycles. The dimensions of the cuboid were measured using a calliper. The procedure was repeated six times on the same sample.

**Fluorescein Encapsulation and Release:** 30 mg of composites <sup>0.30</sup>PBol were immersed and gently mixed for one night with 10 mL of a solution of fluorescein at 1 mM. After removal of the composites, the remaining supernatants were measured by UV spectroscopy to define the encapsulated amount of fluorescein. Standard curve with calibrated solutions (5–20 μM) was established for fluorescein in water, its maximum absorption wavelength being measured at 490 nm. Fluorescein releases from <sup>0.30</sup>PBol were performed by placing composites in 10 mL of water for 10 min with local irradiation with a laser at 808 nm or without irradiation. The amounts of released fluorescein in both cases were then determined by UV spectroscopy.

**Mechanical Characterization:** Mechanical performances were measured by rheology using a MH MARS thermofisher (Germany) and compression tests using an Instron 3366L5885 instrument. Compression test had been performed on cylindrical samples fabricated by stereolithography (8 × 4 mm) and immersed in water for 2 days before testing. The compression test was performed at a speed of 1 mm min<sup>-1</sup> using a 100

N force cell. The compressive strain was expressed as a percentage of the length. Measurements were represented by the mean  $\pm$  standard deviation ( $n = 3$ ). Rheology was performed on cylindrical samples fabricated by stereolithography ( $8 \times 1$  mm) and immersed in water for 2 days before testing. Mechanical properties of the hydrogel were assessed using a parallel (PP 25 sandblasted) plate geometry. Compression force was fixed at 0.2 N and the frequency sweeps were done at 5% constant deformation and recorded between 0.1 and 10 rad  $s^{-1}$ .

## Supporting Information

Supporting Information is available from the Wiley Online Library or from the author.

## Acknowledgements

T.P. and T.B. contributed equally to this work. The authors thank the CNRS, UM, and ENSCM for financial support and the Plateforme d'Analyse et de Caractérisation Balard. T.P. thanks the Ecole Normale Supérieure de Lyon for the PhD funding (CDSN).

## Conflict of Interest

The authors declare no conflict of interest.

## Data Availability Statement

The data that support the findings of this study are available in the Supporting Information of this article.

## Keywords

4D printing, light induced polymerization, nanoparticles, poly(N-isopropylacrylamide), Prussian blue, stereolithography, thermo-responsive hydrogels

Received: August 31, 2023

Revised: October 23, 2023

Published online:

- [1] J. Liu, L. Jiang, S. He, J. Zhang, W. Shao, *Chem. Eng. J.* **2022**, *433*, 133496.
- [2] X. Xu, Y. Liu, W. Fu, M. Yao, Z. Ding, J. Xuan, D. Li, S. Wang, Y. Xia, M. Cao, *Polymers* **2020**, *12*, 580.
- [3] K. Nagase, M. Yamato, H. Kanazawa, T. Okano, *Biomaterials* **2018**, *153*, 27.
- [4] Y. Cheng, C. Huang, D. Yang, K. Ren, J. Wei, *J. Mater. Chem. B* **2018**, *6*, 8170.
- [5] J. Zhao, Y. Ma, N. F. Steinmetz, J. Bae, *ACS Macro Lett.* **2022**, *11*, 961.
- [6] M. A. Haq, Y. Su, D. Wang, *Mater. Sci. Eng., C* **2017**, *70*, 842.
- [7] Y. Guo, J. A. Belgodere, Y. Ma, J. P. Jung, B. Bharti, *Macromol. Rapid Commun.* **2019**, *40*, 1900191.
- [8] H. Zhao, Y. Huang, F. Lv, L. Liu, Q. Gu, S. Wang, *Adv. Funct. Mater.* **2021**, *31*, 2105544.
- [9] Y. Chen, W. Wu, J. Yu, Y. Wang, J. Zhu, Z. Hu, *J. Biomater. Sci., Polym. Ed.* **2020**, *31*, 1770.
- [10] Z. J. Wang, C. Y. Li, X. Y. Zhao, Z. L. Wu, Q. Zheng, *J. Mater. Chem. B* **2019**, *7*, 1674.
- [11] X. Peng, T. Liu, C. Jiao, Y. Wu, N. Chen, H. Wang, *J. Mater. Chem. B* **2017**, *5*, 7997.
- [12] L. Zhang, X. Zhang, L. Li, Y. Liu, D. Wang, L. Xu, J. Bao, A. Zhang, *Macromol. Mater. Eng.* **2020**, *305*, 1900718.
- [13] L.-H. Yu, X. Tao, S.-R. Feng, J.-T. Liu, L.-L. Zhang, G.-Z. Zhao, G. Zhu, *Tungsten* **2022**, <https://doi.org/10.1007/s42864-022-00181-2>.
- [14] J. W. Seo, S. R. Shin, Y. J. Park, H. Bae, *Tissue Eng. Regen. Med.* **2020**, *17*, 423.
- [15] D. Han, C. Farino, C. Yang, T. Scott, D. Browe, W. Choi, J. W. Freeman, H. Lee, *ACS Appl. Mater. Interfaces* **2018**, *10*, 17512.
- [16] Z. Ji, C. Yan, B. Yu, X. Zhang, M. Cai, X. Jia, X. Wang, F. Zhou, *Adv. Mater. Technol.* **2019**, *4*, 1800713.
- [17] S. Miao, H. Cui, M. Nowicki, L. Xia, X. Zhou, S.-J. Lee, W. Zhu, K. Sarkar, Z. Zhang, L. G. Zhang, *Adv. Biosyst.* **2018**, *2*, 1800101.
- [18] C. Cvetkovic, R. Raman, V. Chan, B. J. Williams, M. Tolish, P. Bajaj, M. S. Sakar, H. H. Asada, M. T. A. Saif, R. Bashir, *Proc. Natl. Acad. Sci. USA* **2014**, *111*, 10125.
- [19] D. Han, Z. Lu, S. A. Chester, H. Lee, *Sci. Rep.* **1963**, *8*, 2018.
- [20] B. Singh, A. Indra, *Mater. Today Energy* **2020**, *16*, 100404.
- [21] M. J. P. Muñoz, E. C. Martínez, *Prussian Blue Based Batteries*, Springer, Cham **2018**.
- [22] B. Kong, C. Selomulya, G. Zheng, D. Zhao, *Chem. Soc. Rev.* **2015**, *44*, 7997.
- [23] D. R. Rosseinsky, R. J. Mortimer, in *Electrochromic Materials and Devices* (Eds: R. J. Mortimer, D. R. Rosseinsky, P. M. S. Monk), John Wiley & Sons, Ltd, Hoboken, NJ **2013**, p. 41.
- [24] D. R. Talham, M. W. Meisel, *Chem. Soc. Rev.* **2011**, *40*, 3356.
- [25] S. P. Moulik, G. C. De, A. K. Panda, B. B. Bhowmik, A. R. Das, *Langmuir* **1999**, *15*, 8361.
- [26] S. Vaucher, M. Li, S. Mann, *Angew. Chem., Int. Ed.* **2000**, *39*, 1793.
- [27] X. Wang, L. Cheng, *Coord. Chem. Rev.* **2020**, *419*, 213393.
- [28] Y. Li, J. Hu, K. Yang, B. Cao, Z. Li, L. Yang, F. Pan, *Mater. Today Energy* **2019**, *14*, 100332.
- [29] M. B. Zakaria, T. Chikow, *Coord. Chem. Rev.* **2017**, *352*, 328.
- [30] L. Catala, T. Mallah, *Coord. Chem. Rev.* **2017**, *346*, 32.
- [31] Y. Guari, M. Cahu, G. Félix, S. Sene, J. Long, J. Chopineau, J.-M. Devoisselle, J. Larionova, *Coord. Chem. Rev.* **2022**, *461*, 214497.
- [32] J. Larionova, Y. Guari, C. Sangregorio, C. Guérin, *New J. Chem.* **2009**, *33*, 1177.
- [33] X. Cai, X. Jia, W. Gao, K. Zhang, M. Ma, S. Wang, Y. Zheng, J. Shi, H. Chen, *Adv. Funct. Mater.* **2015**, *25*, 2520.
- [34] S. B. G. Blanquer, M. Werner, M. Hannula, S. Sharifi, G. P. R. Lajoinie, D. Eglin, J. Hyttinen, A. A. Poot, D. W. Grijpma, *Biofabrication* **2017**, *9*, 025001.
- [35] S. B. G. Blanquer, D. W. Grijpma, in *Computer-Aided Tissue Engineering: Methods and Protocols* (Eds.: A. Rainer, Ed., L. Moroni), Springer US, New York, NY **2021**, p. 19.
- [36] J. Huang, Q. Qin, J. Wang, *Processes* **2020**, *8*, 1138.
- [37] L. M. A. Ali, E. Mathlouthi, M. Kajdan, M. Daurat, J. Long, R. Sidi-Boulouar, M. Cardoso, C. Goze-Bac, N. Amdouni, Y. Guari, J. Larionova, M. Gary-Bobo, *Photodiagn. Photodyn. Ther.* **2018**, *22*, 65.
- [38] G. Maurin-Pasturel, E. Rascol, M. Busson, S. Sevestre, J. Lai-Kee-Him, P. Bron, J. Long, J. Chopineau, J.-M. Devoisselle, Y. Guari, J. Larionova, *Inorg. Chem. Front.* **2017**, *4*, 1737.
- [39] E. Mamontova, M. Daurat, J. Long, A. Godefroy, F. Salles, Y. Guari, M. Gary-Bobo, J. Larionova, *Inorg. Chem.* **2020**, *59*, 4567.
- [40] A. Gotoh, H. Uchida, M. Ishizaki, T. Satoh, S. Kaga, S. Okamoto, M. Ohta, M. Sakamoto, T. Kawamoto, H. Tanaka, M. Tokumoto, S. Hara, H. Shiozaki, M. Yamada, M. Miyake, M. Kurihara, *Nanotechnology* **2007**, *18*, 345609.
- [41] B. Zargar, A. Hatamie, *Anal. Methods* **2014**, *6*, 5951.
- [42] F. Lan, J. Bai, H. Wang, *RSC Adv.* **2018**, *8*, 16866.
- [43] D. M. Solis, A. Czekanski, *Soft Matter* **2022**, *18*, 3422.
- [44] B. Sun, Y. Lin, P. Wu, *Appl. Spectrosc.* **2007**, *61*, 765.

- [45] B. Huang, M. Liu, C. Zhou, *Carbohydr. Polym.* **2017**, *175*, 689.
- [46] C. Belda Marín, C. Egles, V. Humblot, Y. Lalatonne, L. Motte, J. Landoulsi, E. Guénin, *ACS Biomater. Sci. Eng.* **2021**, *7*, 2358.
- [47] J. Cho, M. S. Joshi, C. T. Sun, *Compos. Sci. Technol.* **2006**, *66*, 1941.
- [48] T. S. Tran, R. Balu, S. Mettu, N. Roy Choudhury, N. K. Dutta, *Pharmaceuticals* **2022**, *15*, 1282.
- [49] S. Zu, Z. Wang, S. Zhang, Y. Guo, C. Chen, Q. Zhang, Z. Wang, T. Liu, Q. Liu, Z. Zhang, *Mater. Today Chem.* **2022**, *24*, 100789.